Supporting Information

Bifunctional two-dimensional BiPd electrocatalyst for efficient paired CO_2 reduction and ethylene glycol oxidation

Shengqi Yang,[a] Tong Xu,[a] Ruoyin Wang,[a] Yuxin Chen,[a] Feng Yu,*[b] Leiduan Hao*[a] and Zhenyu Sun*[a]

[a] State Key Laboratory of Organic-Inorganic Composites, College of Chemical Engineering, Beijing University of Chemical Technology, Beijing 100029, China. Email: haold@buct.edu.cn; sunzy@buct.edu.cn.

[b] School of Chemistry and Chemical Engineering/State Key Laboratory Incubation Base for Green Processing of Chemical Engineering, Shihezi University, Shihezi 832003, P. R. China. Email: yufeng05@mail.ipc.ac.cn.

Experimental Section

Chemicals and materials

Hexacarbonyl tungsten ($W(CO)_6$), bismuth (III) acetate ($C_6H_9BiO_6$), acetic acid ($C_2H_4O_2$), palladium (II) acetate ($C_4H_6O_4Pd$), N,N-dimethylformamide (DMF), sodium borohydride ($NaBH_4$), Palladium(II) chloride ($PdCl_2$) and bismuth(III) nitrate pentahydrate ($Bi(NO_3)_3.5H_2O$) were purchased from Shanghai Aladdin Bio-Chem Technology Co. Potassium bicarbonate ($KHCO_3$), potassium hydroxide (KOH), isopropanol (C_3H_8O), ethylene glycol ($C_2H_6O_2$), glycolic acid ($C_2H_4O_3$), and D_2O were obtained from Beijing Innochem Science & Technology Co., Ltd. Polytetrafluoroethylene (PTFE)-hydrophobized carbon paper (CP, Toray, YLS-30T GDL) and Nafion D-521 dispersion (5% w/w in water and 1-propanol) were purchased from Alfa Aesar China Co., Ltd. Ar (99.999%) and CO_2 (99.999%) were bought from Beijing Haipu Gas Co., Ltd. Ultrapure water (18.2 MΩ•cm) was obtained from a Millipore system for preparing the sample solutions, electrolytes, and for washing. All chemicals were analytical grade and used without further purification.

Synthesis of BiPd-2D

First, 160 mg of $W(CO)_6$, 77.22 mg (0.2 mmol) of $C_6H_9BiO_6$ and 44.9 mg (0.2 mmol) of $C_4H_6O_4Pd$ were dissolved in 48 mL of DMF. After thorough homogenization, 12 mL of $C_2H_4O_2$ was injected into the mixture, followed by a gentle mixing to form a homogeneous solution. The resulting solution was then transferred into a glass flask to perform the solvothermal reaction at 160 °C for 3 h. At the end of the reaction, the obtained sample was collected by centrifugation at 8000 rpm, washed with deionized water and anhydrous ethanol for three times respectively, and finally dried under vacuum at 60 °C overnight for characterization. The samples with different Bi to Pd ratios was synthesized with the same method with changing molar ratio of $C_6H_9BiO_6$ and $C_4H_6O_4Pd$.

Synthesis of BiPd-NP

Using $NaBH_4$ as the reducing agent, a PdBi catalyst was synthesized via a direct one-step co-reduction reaction of $Bi(NO_3)_3$ and $PdCl_2$. In the typical synthesis of the PdBi catalyst, a 2.5 M $NaBH_4$ solution (5 mL) was rapidly added to a 15 mL solution containing 0.5 mmol $Bi(NO_3)_3$ and 0.5 mmol $PdCl_2$ until no further bubbles formed. The resulting precipitate was washed three times with deionized water and three times with ethanol. The catalyst powder was then vacuum

dried overnight at 60 °C.

Synthesis of BiPd

To prepare BiPd, $Bi(NO_3)_3$•$5H_2O$ (218.4 mg, 0.45 mmol) was first dissolved in HNO_3 solution (12 mL, 1 M), then PVP (180 mg, Mw=1000) and EG (30 mL) were injected into this solution, followed by a vigorous stirring for 30 min. subsequently, $C_4H_6O_4Pd$ (101.03 mg, 0.45 mmol) was added into the mixed solution. After stirring for another 30 min, the solution was transferred into a Teflon-lined stainless-steel autoclave to perform solvothermal process at 150 °C for 12 h. At the end of reaction, the obtained sample was collected by centrifugation, washing with ethanol and finally being dried at 60 °C for characterization.

Material characterization

Powder X-ray diffraction (XRD) patterns were obtained using a D/MAX-RC diffractometer operated at 30 kV and 100 mA with Cu Kα radiation (λ = 0.15418 nm) at a scanning rate of 5° min^{-1}. X-ray photoelectron spectroscopy (XPS) experiments were conducted using a Thermo Scientific ESCALAB 250Xi instrument. The instrument was equipped with an S5 electron flood and a scanning ion gun. The binding energy was corrected for surface charging by referencing the C 1s peak of contaminant carbon at 284.8 eV. Spectral fitting was performed using the XPS Peak41 program with Gaussian functions after subtracting a Shirley background. Scanning electron microscopy (SEM) was performed using an S-4800 microscope with a 3 kV accelerating voltage. Transmission electron microscopy (TEM) and high-resolution TEM (HR-TEM) were conducted on a JEOL ARM200 microscope with a 200kV accelerating voltage. Electrochemical active surface area (ECSA) was obtained from the double-layer capacitance (C_{dl}) value via the equation ECSA = C_{dl}/C_s, where Cs (0.04 mF cm^{-2}) corresponds to the specific capacitance on the surface of the electrode. To calculate the C_{dl} value, cyclic voltammetry (CV) measurements were conducted at different scan rates (10, 20, 40, 60 and 80 mV s^{-1}). In situ EIS investigations were conducted in the frequency range of 100 kHz-0.1 Hz at various potentials.

Preparation of electrodes

The catalyst ink was prepared by ultrasonic dispersion of 12 mg of the catalyst powder with 24 μL Nafion solution (5 wt %) in 2.4 mL isopropanol for 10 min. The prepared ink droplets were then applied to the surface of hydrophobic carbon fiber paper (Toray YLS-30T GDL) to achieve a catalyst loading of 1.0 mg/cm^2. Ordinary Toray carbon paper was used for the electrochemical

oxidation test of ethylene glycol, with all other conditions identical. The electrodes were dried in air before subsequent electrochemical testing.

Electrocatalytic CO_2 reduction

Electrochemical studies were conducted in an electrochemical flow cell comprising a gas chamber, a cathode chamber, and an anode chamber. An anion exchange membrane (Fumasep FAA-3-PK-130) isolated the anode chamber from the cathode chambers, and an Ag/AgCl electrode (3.5 M KCl used as the filling solution) and platinum sheet were used as the reference and counter electrodes, respectively. Electrolysis was performed using a CHI 760E electrochemical workstation equipped with a CHI 680c high-current amplifier. All potentials were converted to reversible hydrogen electrode (RHE) scale according to the formula $E_{RHE} = E_{Ag/AgCl} + 0.197 + 0.059 \times pH$. For performance studies, 1 M KOH was used as the electrolyte, circulated to the cathode and anode chambers at a flow rate of 5 mL/min via a peristaltic pump. The flow rate of carbon dioxide gas through the gas chamber was controlled at 40 sccm using a digital gas flow controller.

Ethylene glycol (EG) electrooxidation

At room temperature, the EG oxidation reaction was conducted in an H-type cell using an electrochemical workstation (CHI 660E, CH Instrument) with a proton exchange membrane (Nafion 117) as the separator. A catalyst-coated carbon paper was employed as the working electrode, a platinum mesh as the counter electrode, and a Hg/HgO electrode as the reference electrode. The cathode electrolyte was 1 M KOH, while the anode electrolyte consisted of a mixture of 1 M ethylene glycol and 1 M KOH. The catalyst loading on the carbon paper was 1 mg/cm^2. The electrochemical oxidation performance of the catalyst toward ethylene glycol was evaluated by measuring i-t curves via the amperometric method for 2 hours at different potentials. The products were analyzed by nuclear magnetic resonance (NMR).

Gaseous and liquid products analysis

The gaseous product in the electrochemical experiment was collected by using a gas bag and analyzed by gas chromatography (Agilent 7890B). The liquid products were quantified using nuclear magnetic resonance spectroscopy (^{1}H NMR). ^{1}H NMR spectra of freshly acquired samples were collected on a Bruker Avance III 400 HD spectrometer. Typically, 300 μL of the electrolyte was mixed with 300 μL of D_2O, and DMSO was used as the interval standard.

The Faradaic efficiency (FE) of the product is:

$$\mathrm{FE} = \frac{Z \times n \times F}{Q_{\mathrm{total}}}$$

FE: faradaic efficiency for Formate, CO or H_2;

Z: number of electrons transferred (Z = 2 for Formate, CO and H_2 production);

n: number of moles for a given product;

F: Faraday's constant (96485 C mol^{-1});

Q_{total}: Where Q_{total} is the total charge passed through the electrodes.

The Faraday efficiency (%) of glycolic acid can be determined through the following equations respectively.

$$\mathrm{FE} = \frac{Z \times n \times F}{Q_{\mathrm{total}}}$$

Z: number of electrons transferred (Z = 4);

n: number of moles for a given product;

F: Faraday's constant (96485 C mol^{-1});

Q_{total}: Where Q_{total} is the total charge passed through the electrodes.

The productivity of glycolic acid formation can be determined by the following equations respectively.

$$GA\ production\ rate\ =\cdot \frac{Moles\ of\ the\ obtained\ GA}{t \times electrode\ area}$$

Energy analysis method

The reduction in the power consumption associated to the electrolysis was calculated based on the difference between the total energy consumption of ECR-OER ($E_{ECR\text{-}OER}$) and ECR-EGOR ($E_{ECR\text{-}EGOR}$) full cell configurations. All values were obtained from the polarization curve of the corresponding electrochemical device. Therefore, the operational energy saving was determined by the following equation: [1]

$$Operational\ energy\ saving\ = \frac{E_{ECR-OER}\ -\ E_{ECR-EGOR}}{E_{ECR-OER}} \times 100\%$$

in which $E_{ECR\text{-}OER}$ and $E_{ECR\text{-}EGOR}$ (J) were calculated based on the following equation:

$$E = I \times U \times t$$

Where I is the current (A), U is cell potential (V) and t is the electrolysis time (second).

Energy efficiency (EE) reflects the efficiency of converting electrical energy into chemical energy, and the calculation formula is: [2]

$$EE = \frac{U_{rev}}{U_{cell}} \times FE_{formate} \times FE_{GA}$$

U_{rev} can be obtained by subtracting the standard electrode potentials of the anode and cathode. The thermodynamic potential of formate is −0.199 V vs RHE, and the thermodynamic potential of GA is 0.57 V vs RHE [3]. U_{cell} is the actual electrolytic cell voltage reading from the polarization curve.

Supplementary Figures

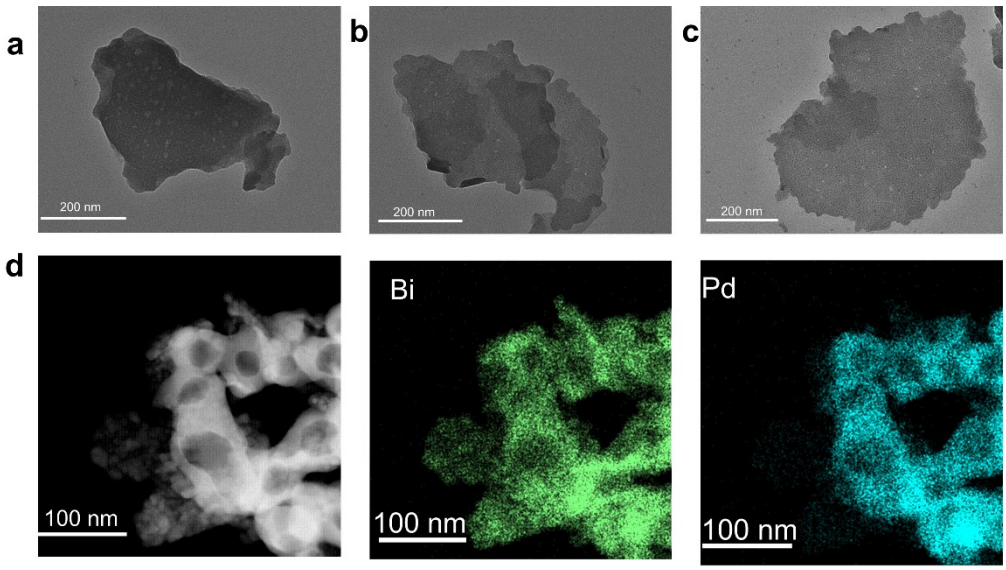

Figure S1 TEM images of a) BiPd-2D, b) BiPd-2D with a Bi to Pd molar ratio of 1:2, and c) BiPd-2D with a Bi to Pd molar ratio of 2:1. d) EDX element mapping of BiPd-2D.

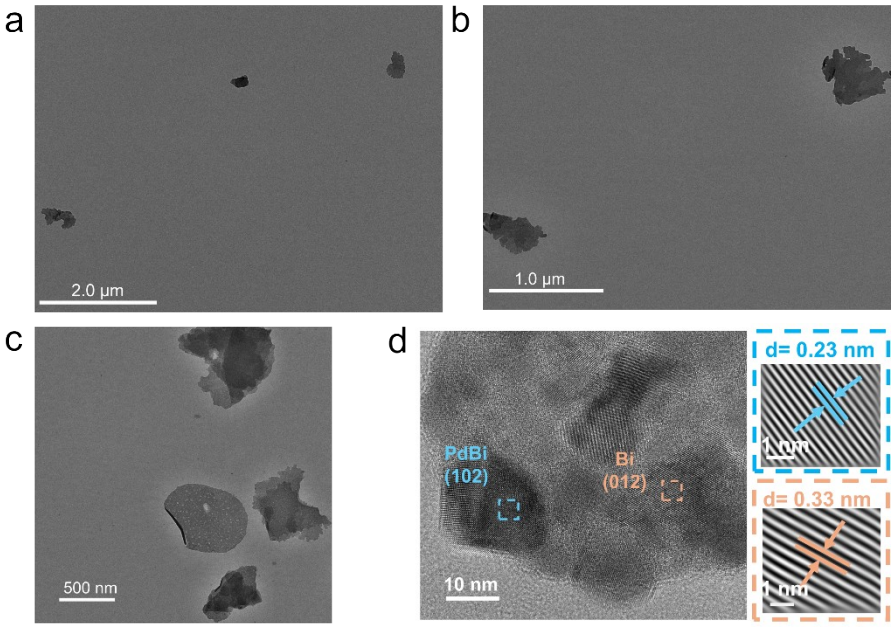

Figure S2 TEM images of BiPd-2D at different magnifications (a-c) showing the predominance of sheet-like nanosheets with a broad lateral-size distribution, typically ranging from hundreds of nanometers to ~1 μm scale. d) HRTEM images of BiPd-2D.

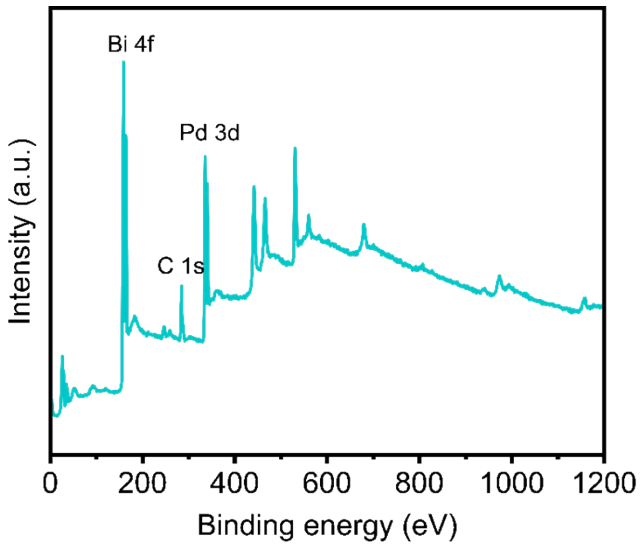

Figure S3 XPS survey spectrum of BiPd-2D.

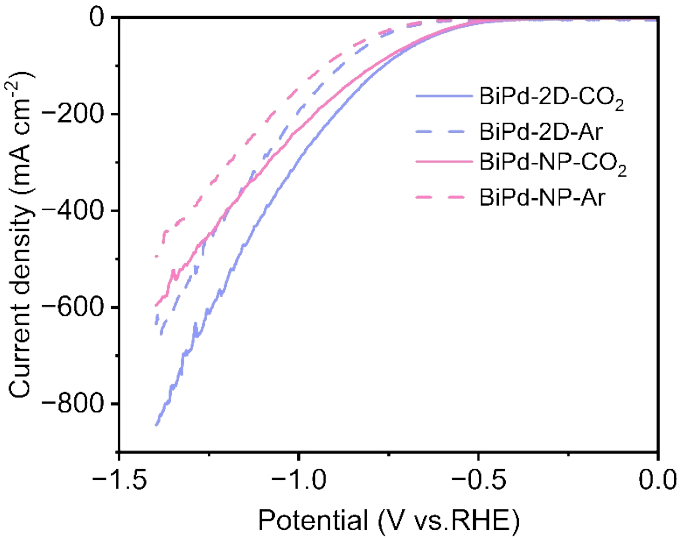

Figure S4 LSV curves over various catalysts conducted in CO_2 and Ar atmosphere.

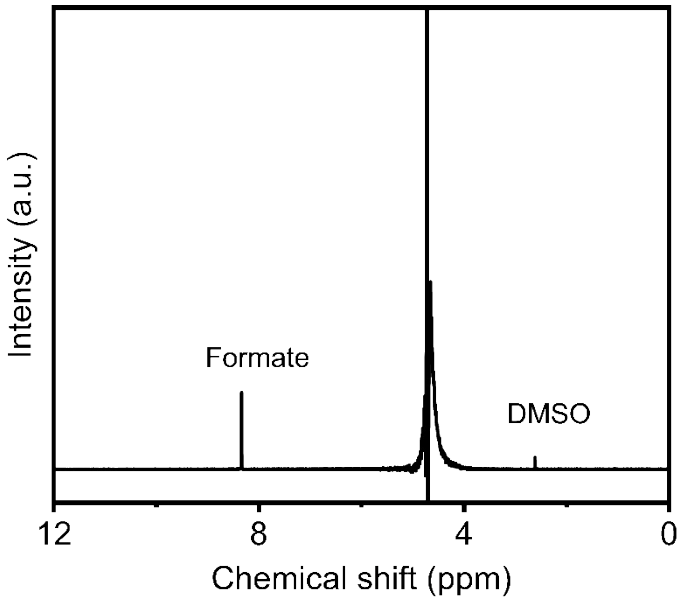

Figure S5 ^{1}H NMR spectrum of the liquid products after ECR.

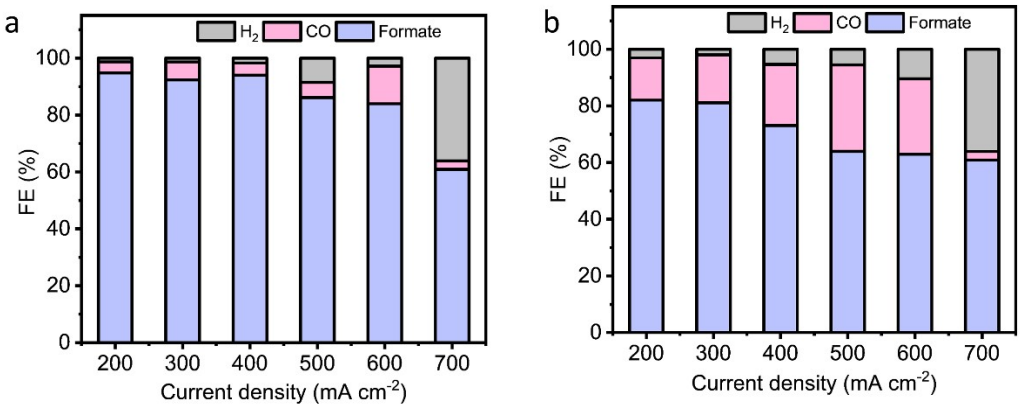

Figure S6 ECR performance of BiPd-2D with a Bi to Pd molar ratio of a) 2:1, and b) 1:2.

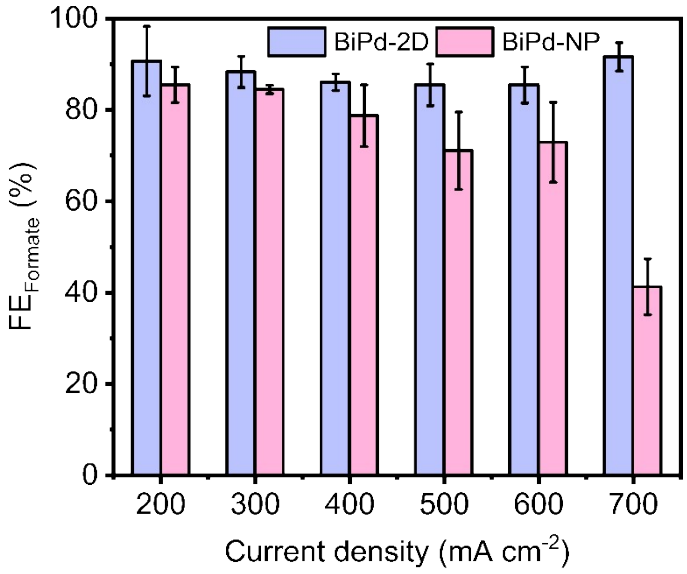

Figure S7 FE of formate for BiPd-2D and BiPd-NP at current densities ranging from 200 to 700 mA cm^{-2}.

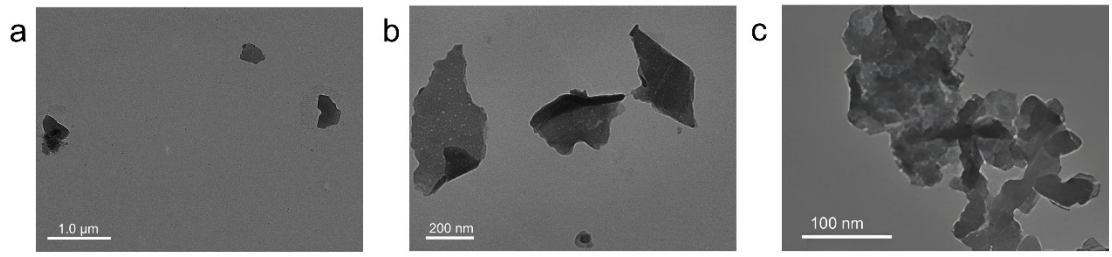

Figure S8 TEM images of a) Bi-2D, b) Pd-2D, and c) BiPd. Bi-2D and Pd-2D exhibit sheet-like morphologies with lateral dimensions in the submicrometer regime. BiPd shows aggregated nanoparticles with primary particle sizes of approximately ~20-60 nm.

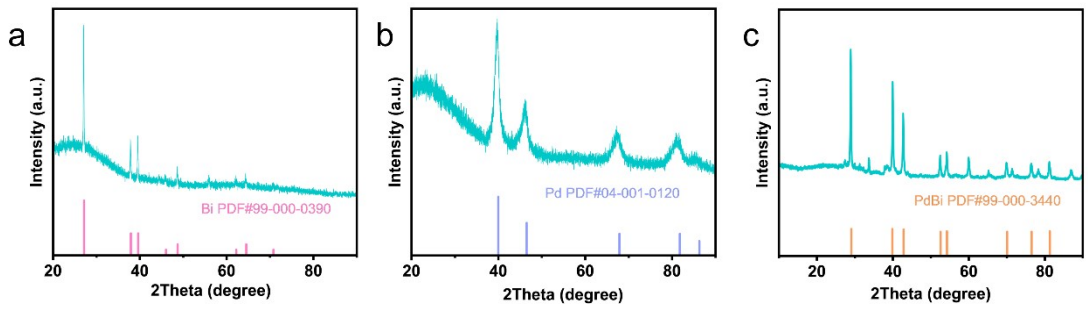

Figure S9 XRD patterns of a) Bi-2D, b) Pd-2D, and c) BiPd.

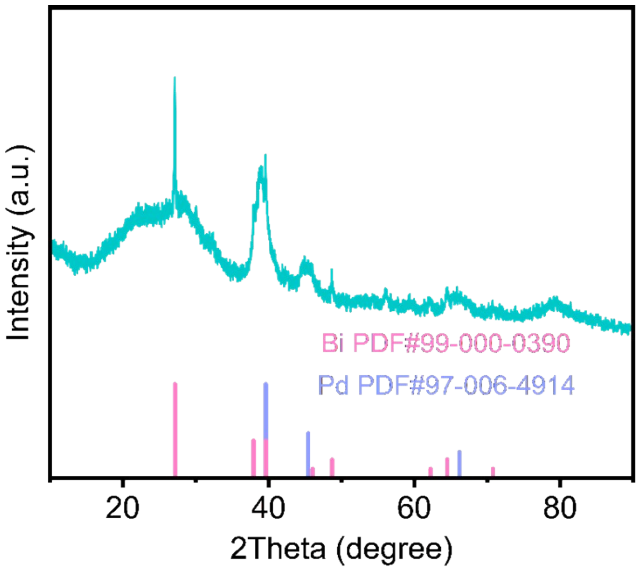

Figure S10 XRD pattern of the BiPd-NP.

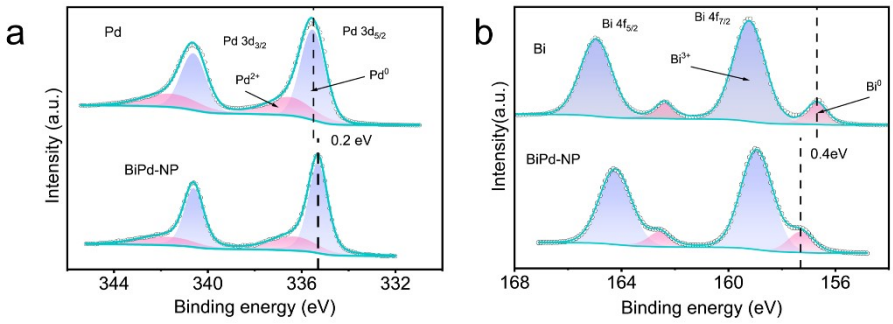

Figure S11 (a) Pd 3d XPS spectrum, (b) Bi 4f XPS spectrum of BiPd-NP.

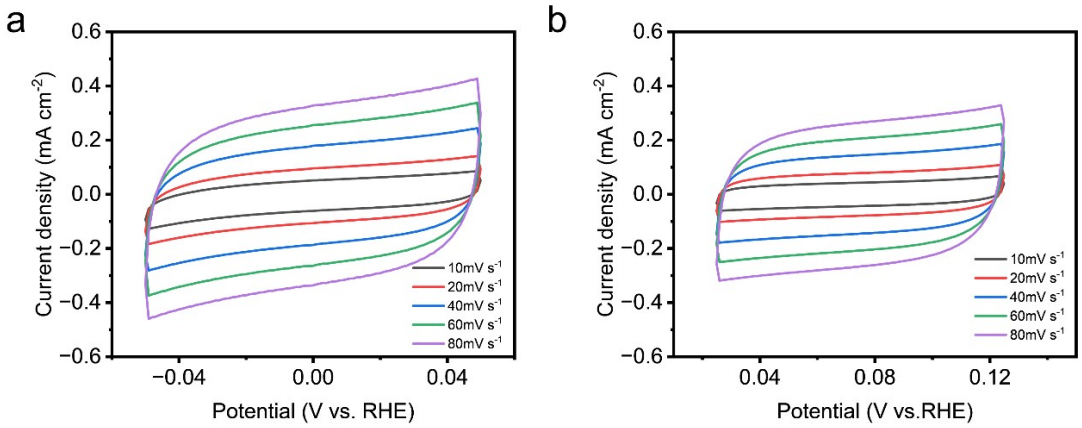

Figure S12 Cyclic voltammograms measured from 10 mV s^{-1} to 80 mV s^{-1} over BiPd-2D (a) and BiPd-NP(b).

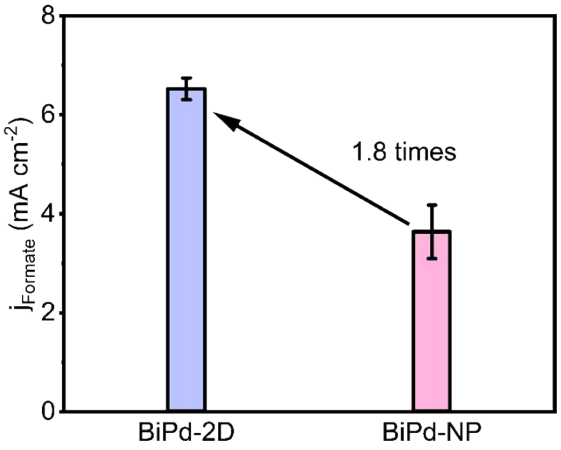

Figure S13 Partial current density of formate normalized to ECSA over BiPd-2D and BiPd-NP at 700 mA cm^{-2}.

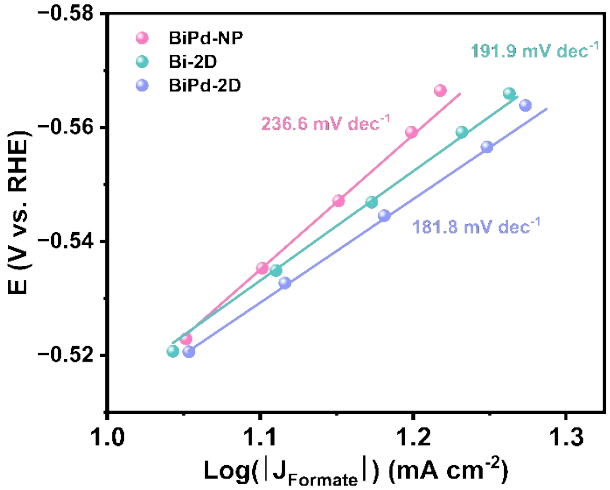

Figure S14 Tafel plots of BiPd-2D, BiPd-NP, and Bi-2D.

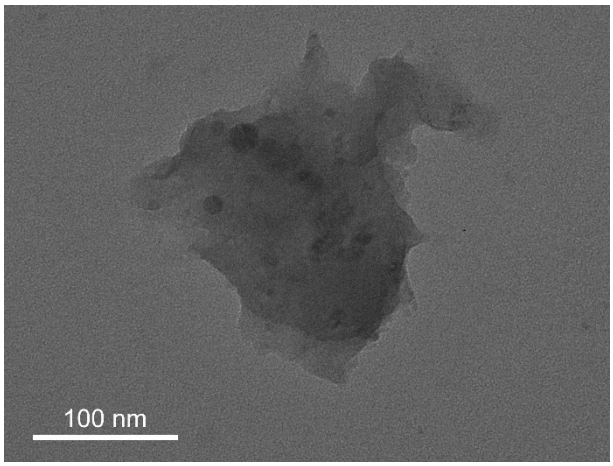

Figure S15 TEM image of BiPd-2D after durability test.

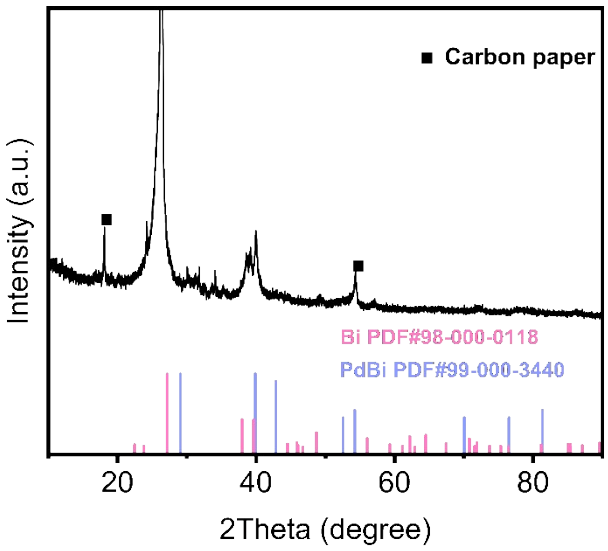

Figure S16 XRD pattern of BiPd-2D after durability test.

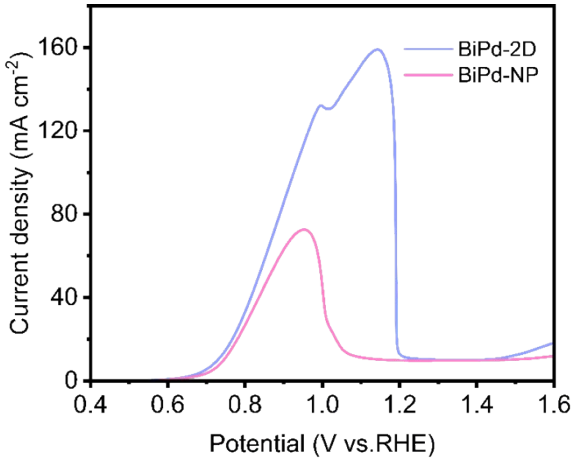

Figure S17 LSV curves of the as-prepared samples in 1 M KOH with 1 M EG.

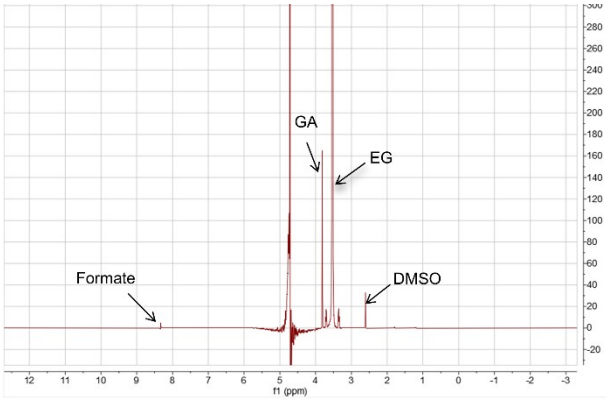

Figure S18 ^{1}H NMR spectrum of electrolyte after EGOR.

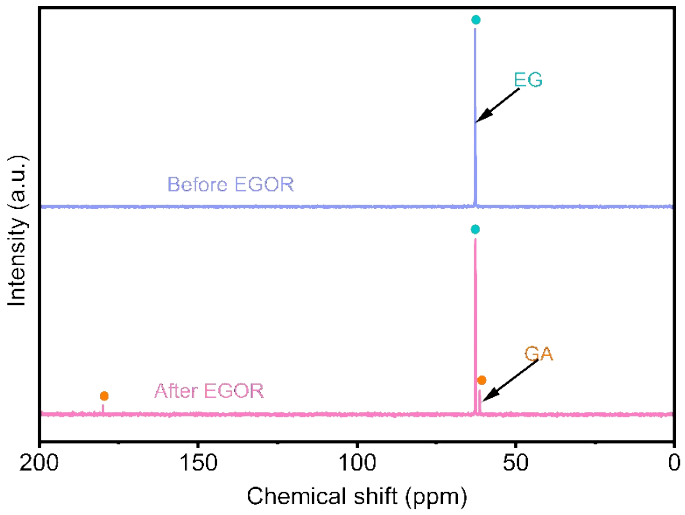

Figure S19 ^{13}C NMR spectra of electrolyte before and after EGOR.

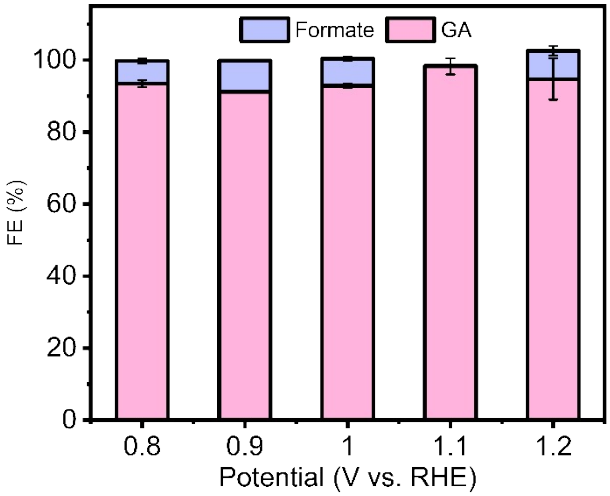

Figure S20 Product distribution of EGOR over BiPd-2D at different potentials.

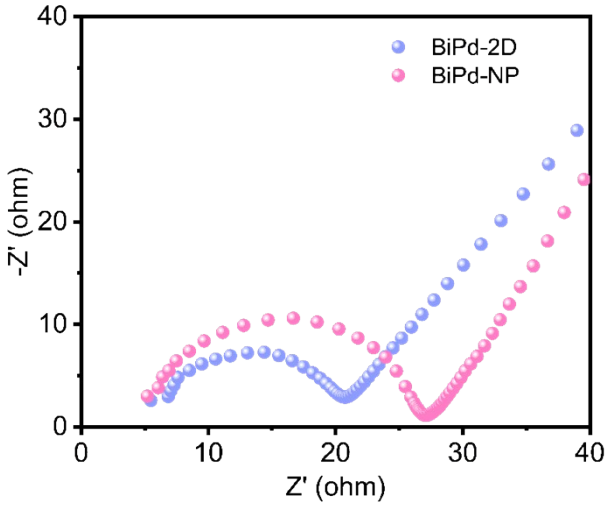

Figure S21 EIS Nyquist profiles of BiPd-2D and BiPd-NP.

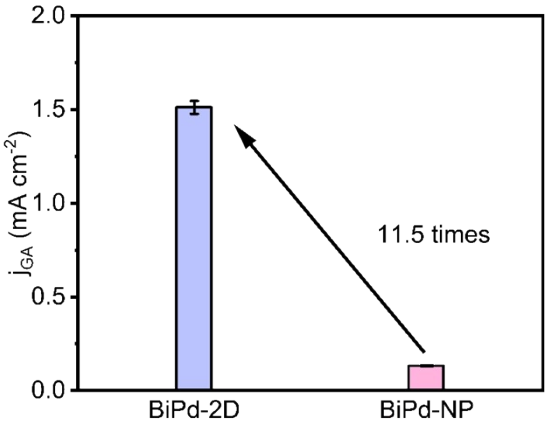

Figure S22 Partial current density of GA normalized to ECSA over BiPd-2D and BiPd-NP at 1.1 V vs. RHE.

Table S1 Elemental analysis for BiPd-2D by ICP-OES

Sample	Element	Reported concentration (ppm)	Atom ratio (Bi:Pd)
BiPd-2D	Bi	5.604	1.5:1
	Pd	1.944	

Table S2 Summary and comparison of recently reported CO_2 paired electrolysis systems.

Electrocatalyst	Reactant	Cell type	Product	current density	Stability	Ref.
BiPd-2D	CO_2, EG	Flow cell	Formate,GA	100 mA cm^{-2}	8 h at 100 mA cm^{-2}	This work
$Ni(OH)_2$ anode 10In-SnO_2/C cathode	CO_2, EG	Flow cell	Formate	20 mA cm^{-2}	0.5 h at 20 mA cm^{-2}	4
NiMn-LDH anode $InO_x(OH)_{3-2x}$ cathode	CO_2, EG	Flow cell	Formate	100 mA cm^{-2}	100 h at 100 mA cm^{-2}	5
CoP anode Ag/BOC cathode	CO_2, glycerol	Flow cell	Formate	50 mA cm^{-2}	1 h at 50 mA cm^{-2}	6
NiOOH@Ni_3S_2 anode Bi cathode	CO_2, glycerol	Flow cell	Formate	160 mA cm^{-2}	0.55 h at 160 mA cm^{-2}	7

$Ni(OH)_2$-V_O anode Bi/Bi_2O_3 cathode	CO_2, EG	Flow cell	Formate	100 mA cm^{-2}	4.2 h at 100 mA cm^{-2}	8
NCO-CFP anode BOC-CNT cathode	CO_2, glucose	MEA	Formate	100 mA cm^{-2}	32 h at 100 mA cm^{-2}	9
$CuO@Ni(OH)_2$ anode Pb-SnO cathode	CO_2, EG	Flow cell	Formate	20 mA cm^{-2}	24 h at 20 mA cm^{-2}	10
CoS/Co-N-C	CO_2, HMF	H cell	CO, FDCA	50 mA cm^{-2}	50 h at 50 mA cm^{-2}	11
NiOOH/NF anode Bi_2O_3 cathode	CO_2, EG	MEA	Formate	100 mA cm^{-2}	2 h at 100 mA cm^{-2}	12
NiCo LDHs anode Cu_1Bi cathode	CO_2, HMF	MEA	Formate, FDCA	150 mA cm^{-2}	10 h at 150 mA cm^{-2}	13
CuCoO anode $Bi_2O_2CO_3$ cathode	CO_2, EG	Flow cell	Formate	25 mA cm^{-2}	24 h at 25 mA cm^{-2}	14

1. T.-H.-H. Le, Y. Zuo, M. Chatti, M. Rizzo, A. Griesi, A. Annamalai, S. Lauciello, L. Leoncino, M. Prato, S. Dante, I. Kriegel, G. Divitini, M. Ferri and L. Manna, *Angew. Chem., Int. Ed.*, 2025, **64**, e202502617.
2. V. Trivedi, B. Rajeshwaree, R. Biswas, M. Kashyap, S. Bhattacharya and A. Dutta, *Cell Rep. Phys. Sci.*, 2025, **6**, 102790.
3. Y. Jiang, L. Li, J. Zhang, W. Li, X. Zhao, Y. Xie, M. Guo and M. Zhong, *Chem.-Asian J.*, 2025, **20**, e00685.
4. L. Zhou, Z. Qu, L. Fu and Y. Ding, *Appl. Catal., B*, 2025, **377**, 125471.
5. B. Li, Z. Zhong, H. Li, M. Yue, Q. Niu, L. Liu, W. Xie, M. Li, M. Shao and Q. Wang, *Angew. Chem., Int. Ed.*, 2025, **64**, e202509502.
6. X. Guo, S.-M. Xu, H. Zhou, Y. Ren, R. Ge, M. Xu, L. Zheng, X. Kong, M. Shao, Z. Li and H. Duan, *ACS Catal.*, 2022, **12**, 10551−10559.
7. D. Chen, S. Yang, J. Gao, X. Zheng, J. Mao, Q. Hu, X. Sun, L. Ji, X. Zheng, H. Fu, W. Xue, H. Chen, S. Li, C. Cheng, J. Peng, X. Jiao, R. Li, M. Grätzel and J. Xu, *Nano Res.*, 2025, **18**, 94907399.
8. F. Ma, Z. Li, R. Hu, Z. Wang, J. Wang, J. Li, Y. Nie, Z. Zheng and X. Jiang, *ACS Catal.*, 2023, **13**, 14163−14172.
9. R. Zhao, Y. Wang, G. Ji, F. Zhang, Y. Wang, Y. Zhao, B. Han and Z. Liu, *Chem. Eng. J.*, 2024, **486**, 150280.
10. I. Bashir, J. D. McGettrick, M. F. Kühnel, B. Sarfraz, S. N. Arshad and A. Rauf, *ACS Sustainable Chem. Eng.*, 2024, **12**, 4795−4802.

11. J. Zhang, D. Yan, G. Ding, X. Wang, C. Li, S. Zhong, Y. Yu, L. Shuai and G. Liao, *Angew. Chem., Int. Ed.*, 2025, **64**, e202511448.
12. Y. Fang, C. Cai, H. Yamashita, X. Qian and Y. Zhao, *Catal. Today*, 2026, **462**, 115544.
13. S.-Q. Liu, M.-R. Gao, S. Wu, R. Feng, Y. Wang, L. Cui, Y. Guo, X.-Z. Fu and J.-L. Luo, *Energy Environ. Sci.*, 2023, **16**, 5305−5314.
14. S. K. Kilaparthi, A. Addad, A. Barras, S. Szunerits and R. Boukherroub, *J. Mater. Chem. A*, 2023, **11**, 26075−26085.